Copper complexes as biomimetic models of catechol oxidase: mechanistic studies

Koval, I.A.

7 | Catecholase activity of a μ-hydroxo-dicopper(II) macrocyclic complex: structures, intermediates and reaction mechanism[†]

This chapter reports the catecholase activity of the dicopper(II) complex $[Cu_2([22]py4pz)(\mu\text{-}OH)](ClO_4)_3 \cdot H_2O$ (**1**), as well as the syntheses and characterization of its reduced dicopper(I) analogue $[Cu_2([22]py4pz)](ClO_4)_2 \cdot 2CH_3OH$ (**2**) and the trans-μ-1,2-peroxo-dicopper(II) adduct **3** ([22]py4pz = (9,22-bis(2-pyridylmethyl)-1,4,9,14,17,22,27,28,29,30-decaazapentacyclo-[22.2.1.1^{4,7}.1^{11,14}.1^{17,20}]triacontane-5,7(28),11(29),12,18,20(30),24(27),25-octaene). These three compounds represent models of the three states of the catechol oxidase active site: *met*, *deoxy* (reduced) and *oxy*. The dicopper(II) complex **1** catalyzes the oxidation of catechol model substrates in aerobic conditions, while in the absence of dioxygen a stoichiometric oxidation takes place, leading to the formation of quinone and the dicopper(I) complex. The catalytic reaction follows a Michaelis-Menten behavior. The dicopper(I) complex binds dioxygen at low temperature, forming a trans-μ-1,2-peroxo-dicopper adduct, which has been characterized by UV-Vis and resonance Raman spectroscopy, and electrochemically. This peroxo complex stoichiometrically oxidizes a second molecule of catechol in the absence of dioxygen. A catalytic mechanism of catechol oxidation by **1** has been proposed, and its relevance to the mechanisms earlier proposed for the natural enzyme and other copper complexes is discussed.

[†]This chapter is based on: Koval, I. A., Belle, C., Selmeczi, K., Philouze, C., Saint-Aman, E., Schuitema, A. M., Gamez, P., Pierre, J.-L., Reedijk, J., J. Biol. Inorg. Chem., 2005, 10, 739-750

7.1 Introduction

As discussed in Chapter 1, despite the large number of model complexes reported in the literature,[1-14] the mechanism of the catechol oxidation by the natural enzyme and by the model complexes still remains far from clear. In Chapter 6, the structure of dicopper(II) complex **1** with a macrocyclic ligand [22]py4pz (Scheme 7.1) with a single hydroxo bridge between the copper centers,[15] which is fairly similar to the *met* form of the active site of catechol oxidase, has been reported. Consequently, in order to investigate catechol oxidation mechanism by **1**, its interaction with catechol model substrates in aerobic and anaerobic conditions has been examined, and the results are presented in the present chapter. The structure and the properties of the dicopper(I) complex $[Cu_2([22]py4pz)](ClO_4)_2{\cdot}2CH_3OH$ (**2**), the dioxygen binding by this complex, leading to a trans-μ-1,2-peroxo-dicopper adduct **3,** and the interaction of the latter species with phenol and catechol substrates are also discussed. Based on the results, a mechanism for the catechol oxidation by **1** is proposed, which closely resembles the earlier one proposed by Krebs and co-workers[16] for the natural enzyme, shedding a new light on the oxidation of phenol and catechol substrates by peroxo-dicopper species.

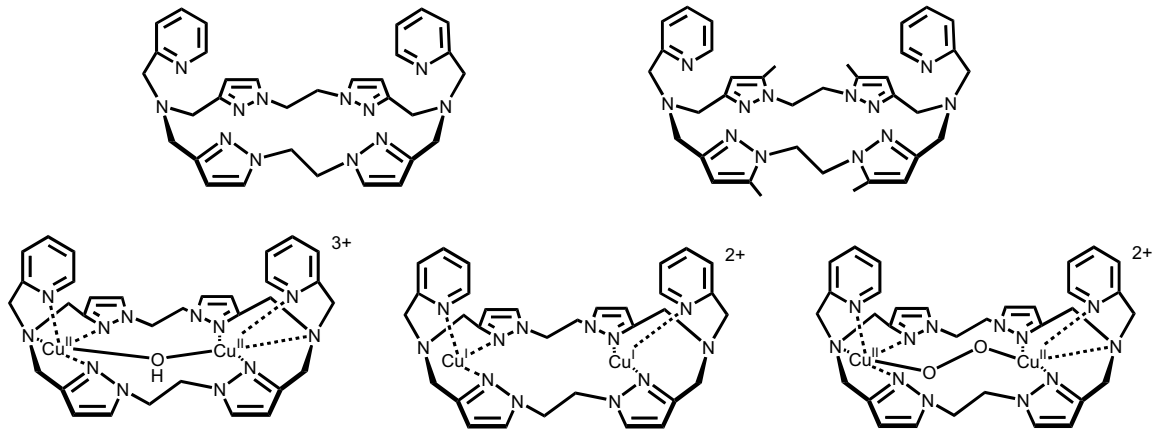

Scheme 7.1. Schematic representations of the ligand [22]py4pz (left, top), its methyl-substituted analog Me[22]py4pz (right, top),[17] the complex cation $[Cu_2([22]py4pz)(\mu\text{-}OH)]^{3+}$ ($\mathbf{1}^{3+}$, left, bottom), the complex cation $[Cu_2([22]py4pz)]^{2+}$ ($\mathbf{2}^{2+}$, middle, bottom) and trans-μ-1,2-peroxo-dicopper adduct $[Cu_2([22]py4pz)(\mu\text{-}O_2)]^{2+}$ ($\mathbf{3}^{2+}$, right, bottom).

7.2 Results and Discussion

7.2.1 Synthesis of the ligand, 1 and 2

The synthesis of the macrocyclic ligand [22]py4pz and the hydroxo-bridged dicopper(II) complex **1** are outlined in Chapter 6. The dicopper(I) complex **2** has been synthesized by reacting $Cu(CH_3CN)_4(ClO_4)$ with [22]py4pz in methanol in dry glove box atmosphere. The diffusion of diethyl ether into the colorless solution, containing two molar equivalents of $Cu(CH_3CN)_4(ClO_4)$ and one equivalent of the ligand, led to the appearance of the small colorless crystals of the product.

7.2.2 Crystal structure description

$[Cu_2([22]py4pz)(\mu\text{-}OH)](ClO_4)_3]\cdot H_2O$ (1)

The crystal structure of **1** has been described in detail in Chapter 6;[15] for clarity it will be very briefly described here. The molecular plot of the complex cation is shown in Figure 6.2 (see Chapter 6). The Cu^{II} ions are in an N_4O environment, which can be best described as distorted trigonal bipyramid ($\tau = 0.83$; $\tau = 0$ for the regular square pyramid and 1 for the regular trigonal bipyramid geometry[18]). The oxygen atom O23 of the hydroxo group bridges two copper ions, occupying the axial position in their coordination spheres and keeping them on a distance of 3.7587(11) Å. The Cu-O-Cu angle is 156.0(3)°.

$[Cu_2([22]py4pz)](ClO_4)_2\cdot 2CH_3OH$ (2)

The molecular structure of **2** is presented in Figure 7.1. Selected bond lengths and angles are given in Table 7.1.

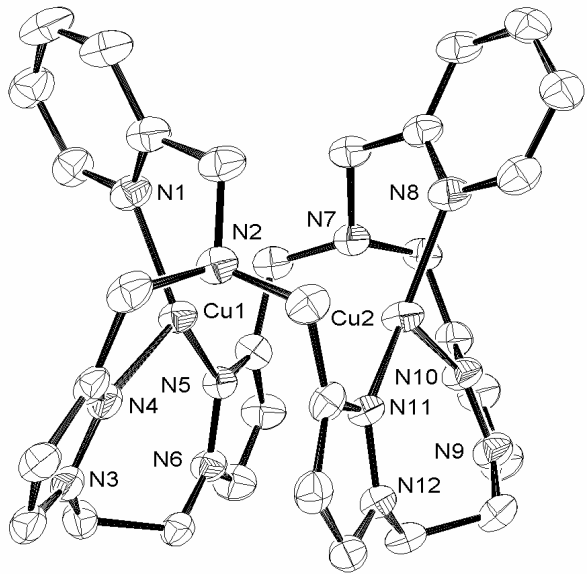

Figure 7.1. ORTEP representation of the complex cation $[Cu_2([22]py4pz)]^{2+}$. Hydrogen atoms are omitted for clarity.

The macrocyclic ligand adopts a saddle-shaped structure with a roof closed by the two pyridines. The complex cation encloses two copper(I) ions at a distance of 3.3922(7) Å, which is shorter than the intermetallic distance in **1**. The Cu1 and Cu2 cations are surrounded by the nitrogen atom of the pyridine ring (N1 and N8 respectively) at an average distance of 2.008 Å and the nitrogen atoms of two pyrazole rings (N4, N5 and N10, N11, respectively) at distances of 2.014(3) (Cu1) or 2.024(3) Å (Cu2) and 1.958(3) (Cu1) or 1.953(3) Å (Cu2), respectively. The tripodal nitrogen atoms (N2 and N7) are located at longer distances of 2.383(4) and 2.407(3) Å. The N-

Cu-N angles around both metal ions range between 76° and 143°. The coordination mode of both copper ions should thus be regarded as trigonal planar rather than tetrahedral, the two tripodal nitrogen atoms being considered as non-coordinating. However, the trigonal planar surrounding is distorted, the coordination angles deviating from the value of 120° expected for a regular trigonal planar geometry. When the oxidation state of a bound metal cation is known unambiguously, the bond valence sum calculation (BVS) can be used to confirm the coordination number.[19] In the present case the value calculated gives a BVS of 1.067 in agreement with a tricoordinated Cu^{I} ion.

Table 7.1. Selected bond lengths and bond angles for $[Cu_2([22]py4pz)](ClO_4)_2 \cdot 2CH_3OH$ (**2**)

Bond distances (Å)			
Cu1 - N1	2.008(3)	Cu2 - N10	2.024(3)
Cu1 - N4	2.014(3)	Cu2 - N11	1.953(3)
Cu1 - N5	1.958(3)	Cu2 - N8	2.008(4)
Cu1 - N2	2.383(4)	Cu2 - N7	2.407(3)
Bond angles (°)			
N1 - Cu1 - N4	112.0(1)	N8 - Cu2 - N10	111.9(1)
N1 - Cu1 - N5	129.7(1)	N8 - Cu2 - N11	130.3(1)
N4 – Cu1 – N5	107.7(1)	N10 – Cu2 – N11	108.1(1)
N5 - Cu1 - N2	143.4(1)	N8 - Cu2 - N7	76.3(1)
N1 - Cu1 - N2	76.6(1)	N10 - Cu2 - N7	77.4(1)
N4 - Cu1 - N2	76.6(1)	N11 - Cu2 - N7	141.8(1)

7.2.3 Formation of trans-*μ*-1,2-peroxo-dicopper(II) complex (3)

Upon dioxygen addition to a solution of **2** in acetonitrile at -40 °C, the UV-Vis spectra of the resulting dark purple solution display two absorption bands at 523 nm (ε = 4320 $M^{-1} \cdot cm^{-1}$) and 617 nm (ε = 2212 $M^{-1} \cdot cm^{-1}$), ascribed respectively to $\pi_\sigma^* \rightarrow$d and $\pi_v^* \rightarrow$d peroxo to Cu^{II} CT transitions,[20,21] which develop almost instantaneously (Figure 7.2, left). The resonance Raman spectrum of the final product **3** (*in situ* formed in acetonitrile) is characterized by two peaks besides the peaks from the solvent (Figure 7.2, right, curve A). The first peak at 510 cm^{-1} was assigned to a ν(Cu-O) stretching, while the second one, at 840 cm^{-1}, corresponds to an intra-peroxide ν(O-O) stretching. These UV-Vis and Raman spectroscopic characteristics are typical for trans-*μ*-1,2-peroxo-dicopper species and suggest that dioxygen is bound to both copper(II) ions in a symmetric end-on fashion,[22] similarly to the earlier reported dicopper-peroxo complex with the macrocyclic ligand Me[22]py4pz (Scheme 7.1),[17] which only differs from the ligand [22]py4pz by the presence of methyl substituents on the pyrazole rings. Numerous studies on the formation of trans-*μ*-1,2-peroxo-dicopper complexes indicate

that oxygenation of the corresponding dicopper(I) complex usually proceeds via formation of an intermediate copper(II)-superoxo Cu-$O_2^{\bullet-}$-species, characterized by an intensive absorption band at *ca.* 410 nm (ε = 3000-8000 $M^{-1}\cdot cm^{-1}$),[22] however, this species has not been observed upon dioxygen addition to **2**.

The formed trans-μ-1,2-peroxo-dicopper(II) complex **3** is stable for *ca.* 3 hours in acetonitrile solution at -40 °C, but less stable than the trans-μ-1,2-peroxo-dicopper(II) complex with Me[22]py4pz, the methyl substituents in the latter ligand apparently sterically protecting the highly reactive peroxo core. Its decomposition leads to the formation of a light-green solution, characterized by a strong absorption band at 350 nm (ε *ca.* 10000 $M^{-1}\cdot cm^{-1}$). This spectrum is consistent with the formation of the μ-hydroxo-bridged dicopper(II) complex **1**.[15,23] This species was further confirmed by ESI-MS studies (m/z 465, z = 2), corresponding to $[[Cu_2([22]py4pz)(\mu\text{-}OH)(CH_3CN)_2(H_2O)]ClO_4]^{2+}$, the isotopic distribution pattern being consistent with the theoretically expected one. As for $[Cu_2(Me[22]py4pz)(\mu\text{-}O_2)]^{2+}$, the dioxygen binding was found to be irreversible, as the absorption of the peaks at 523 and 617 nm did neither diminish upon purging the solution with argon for a few hours, nor by evaporation of the solvent under reduced pressure.

A test assaying the dihydrogen peroxide produced by the addition of an excess of trifluoroacetic acid to the oxygenated solution in acetone at -60 °C, indicated that H_2O_2 was formed in 92% yield, considering a $2Cu{:}1O_2$ stoichiometry.[24]

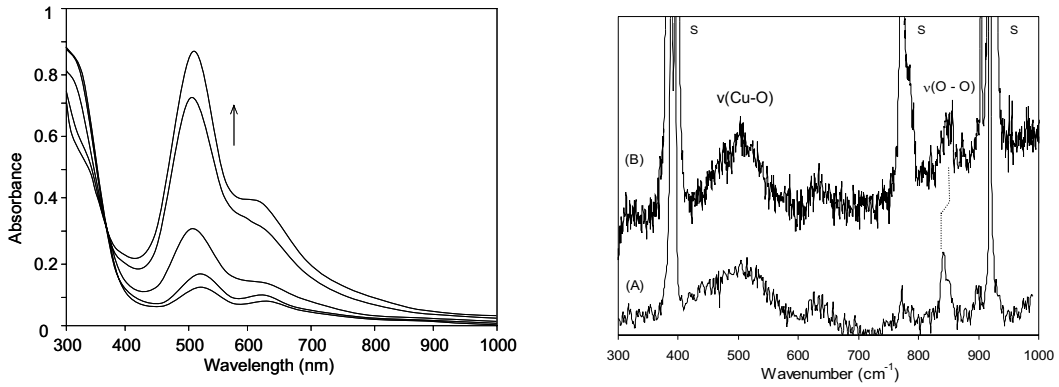

Figure 7.2. Left: changes in the UV-Vis spectrum upon bubbling dioxygen into a 2.5×10^{-4} M solution of **2** (-40 °C, CH_3CN, spectra recorded every 0.2 min). Right: resonance Raman spectrum of **3** (*in situ*, CH_3CN, curve A) and **4** (*in situ*, **3** + 1 eq. 3-FC, CH_3CN, curve B, see Section 7.2.9 for further details), excitation wavelength 514.532 nm; the peaks marked "s" originate from solvent.

7.2.4 General properties of the compounds

The magneto-chemical properties and the NMR spectra of complex **1** have been discussed in Chapter 6.[15] The compound exhibits a very strong antiferromagnetic coupling ($2J$ = -691(35) cm^{-1}) between the copper ions, leading to an EPR-silent complex in both the solid state and in a frozen acetonitrile solution. The complex was found to be moderately soluble in acetonitrile and DMSO, poorly soluble in water, and

completely insoluble in other common solvents. The UV-Vis-NIR spectrum of the complex in CH_3CN solution exhibits two absorption bands at 350 nm (ε = 7176 $M^{-1}\cdot cm^{-1}$) and at 821 nm (ε = 336 $M^{-1}\cdot cm^{-1}$). The first one corresponds to the charge transfer band from the hydroxo bridge to the copper ions, whereas the second one is assigned to the d-d transition band of the Cu^{II} ions.

Complex **2** was found to be moderately soluble in acetonitrile and methanol and very air- and moisture-sensitive. Therefore, it could only be stored in the inert atmosphere of a dry glove box. Its NMR spectrum is characterized by relatively sharp peaks at room temperature and indicates a symmetric structure of the compound in solution.

7.2.5 Acid-base properties of 1

The acid-base properties of **1** have been first studied by spectrophotometric titration of a solution of **1** in a DMSO/water mixture (1:9) with 0.01 M solutions of NaOH and $HClO_4$. A DMSO/water mixture has been used due to the very poor solubility of **1** in pure water. The ionic strength was maintained constant with a 0.01 M solution of $NaNO_3$ (aq) (sodium perchlorate could not be used, as the complex precipitates in the presence of an excess of perchlorate ions in this solvent).

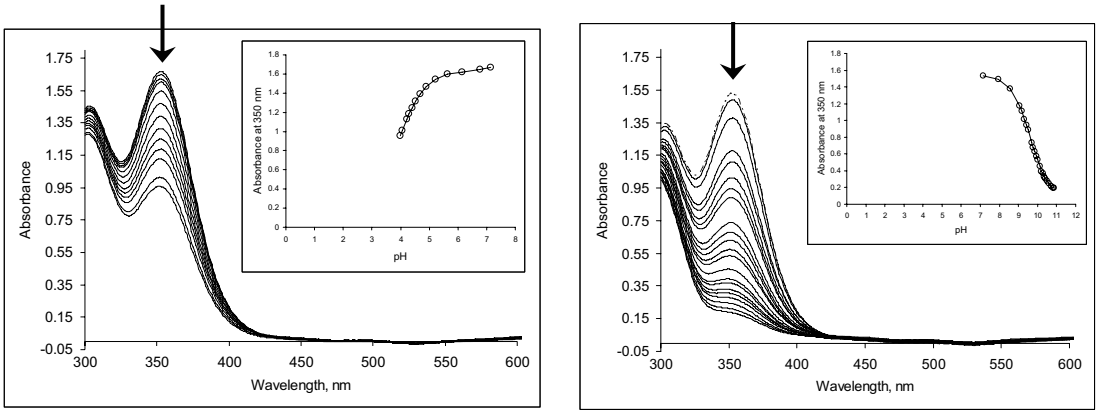

Figure 7.3. Changes in the UV-Vis spectrum of **1** upon titration with $HClO_4$ (left, pH range 7.1 – 4.0) and NaOH (right, pH range 7.1 – 10.9). The insert shows the decrease in absorption of the LMCT band at 350 nm *vs.* pH of the solution.

The titration of **1** by $HClO_4$ results in the progressive diminishing of the CT band at 350 nm till its disappearance at pH 3 (Figure 7.3, left). This process is reversible upon addition of NaOH. A plot of the absorbance *vs.* pH indicates that the protonation process has an apparent pK_1 of 4.0 (±0.05). Similarly, the titration of **1** with NaOH leads to the decrease of the CT band at 350 nm till its complete disappearance at pH 11, with an apparent pK_2 of 9.5 (±0.07) (Figure 7.3, right), and 97% of its initial absorption is restored upon addition of $HClO_4$. No isosbestic points were observed. Thus, the initial structure of **1** is preserved in a limited pH range (pH 5 – 8) and undergoes protonation or deprotonation at higher and lower pH; however, the process is reversible upon restoration of pH to neutral values. This has been further studied from an NMR titration

in a DMSO-d_6/D_2O (1:9) mixture. The NMR resonances of **1** broaden upon addition of either CF_3COOD or NaOD, and their intensity progressively decreases, without any new resonances appearing in the spectrum. The latter results suggest that at higher and lower pH, a dissociation of the hydroxo bridge takes place, leading to the decrease of the antiferromagnetic coupling between the copper(II) centers and signals broadening, and possibly with a subsequent ligand protonation at low pH values.

7.2.6 Electrochemical studies of 1, 2 and 3

The electrochemical behavior of complexes **1** and **2** and the trans-μ-1,2-peroxo adduct **3** (*in situ*) has been investigated by cyclic voltammetry (CV) and rotating disk electrode voltammetry (RDE) in acetonitrile solution, with tetra-*n*-butylammonium perchlorate (TBAP) as supporting electrolyte (0.1 M). The potentials are referred to an Ag/10 mM $AgNO_3$ + CH_3CN + 0.1 M TBAP reference electrode.

The CV curve of complex **1** is characterized by three successive electrochemical signals (Figure 7.4, left) at E_{pc} = -0.43, -0.80 and -1.20 V, respectively. Coulometric titration allows to attribute these systems to the complexed $Cu^{II,II}_2/Cu^{II,I}_2$, $Cu^{II,I}_2/Cu^{I,I}_2$ redox couples and finally to the formation of Cu^0 onto the electrode surface. The first system is quasi-reversible, whereas the second one is irreversible. As previously described,[25] OH^- bridges have a poor ability to bind Cu^I centers and tend to dissociate upon copper reduction, causing the irreversibility of the electrochemical system. These results have been confirmed by rotating disk electrode (RDE) voltammetry experiments (Figure 7.4, right) with two well-behaved cathodic waves at $E_{1/2}$ = -0.45 V and -1.20 V. The third cathodic wave at $E_{1/2}$ = -0.80 V could not be observed due to an adsorption phenomenon.

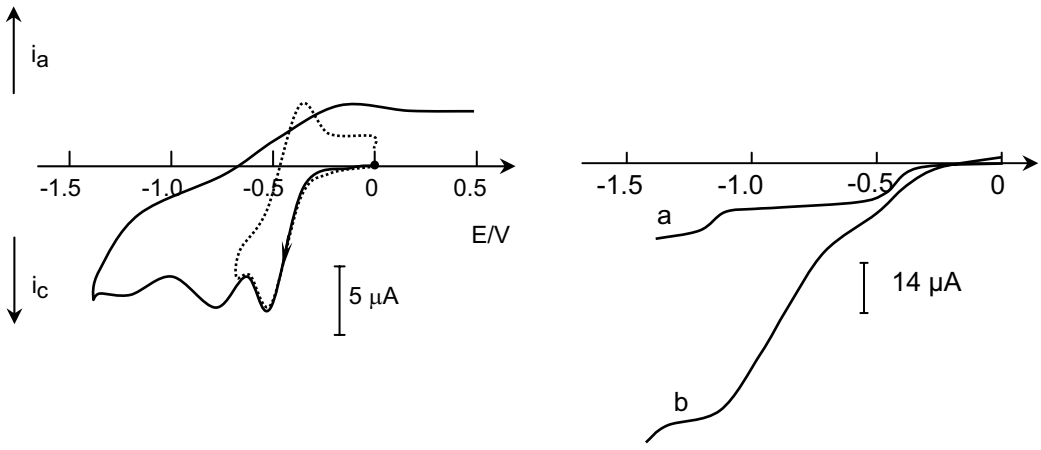

Figure 7.4. Left: CV curves recorded in a 1 mM solution of **1** in CH_3CN + 0.1 M TBAP on a Pt disc (∅ = 5 mm), v = 0.1 $V \cdot s^{-1}$. Right: RDE curves of **1** (curve a) and **1** in the presence of 10 molar equivalents of $DTBCH_2$ (curve b, see Section 7.2.8 for further details), N = 600 rpm; v = 0.01 $V \cdot s^{-1}$; V *vs.* Ag/10 mM $AgNO_3$ + CH_3CN + 0.1 M TBAP.

The anodic part of the CV curve for **2** (Figure 7.5, left) is characterized by one fully irreversible broad electrochemical signal at E_{pa} = +0.18 V, likely resulting from the overlapping of two successive oxidation waves corresponding to the complexed $Cu^{I,I}{}_2/Cu^{II,I}{}_2$ and $Cu^{II,I}{}_2/Cu^{II,II}{}_2$ redox couples. On the reverse scan, a quasi-reversible one-electron reduction peak at $E_{1/2}$ = -0.43 V is observed, which corresponds to the one-electron reduction of the complex **1**, formed upon oxidation of **2**.

The CV curve of **3** (*in situ*), recorded at -40 °C, displays one ill-behaved irreversible reduction wave at E_{pc} = -0.64 V (Figure 7.5, right, curve a). The reduction of molecular dioxygen, present in solution, is observed at -1.0 V, precluding the observation of other cathodic waves.

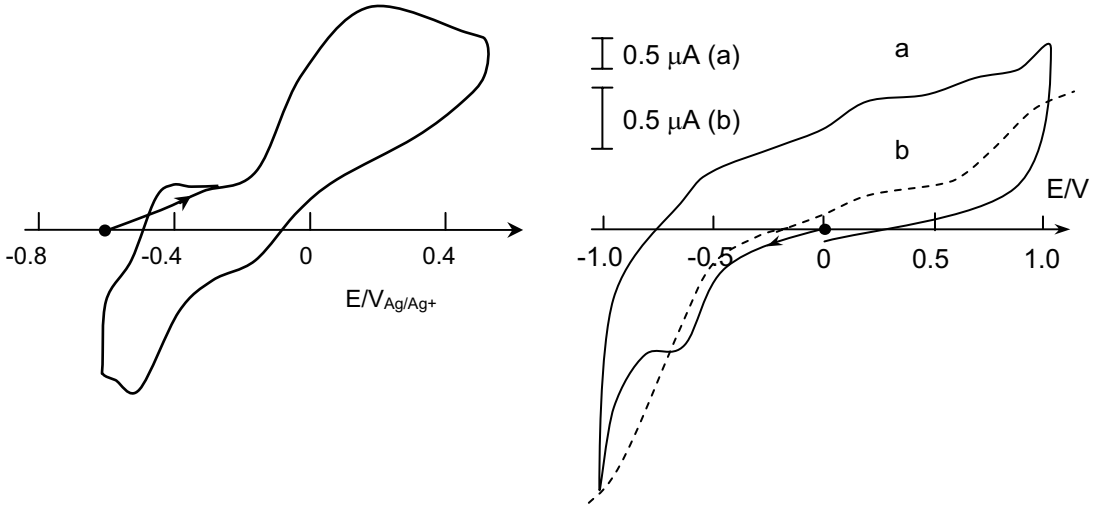

Figure 7.5. Left: CV curve recorded in a 1 mM solution of **2** in CH_3CN + 0.1 M TBAP on a Pt disc (∅ = 5 mm), v = 0.1 $V{\cdot}s^{-1}$. Right: voltammetric curve in CH_3CN + 0.1 M TBAP of the peroxo-dicopper complex **3** (*in situ*, 2.5×10^{-4} M, CH_3CN, -40 °C). (a) CV curve 0.1 $V{\cdot}s^{-1}$ (b) (dotted line) RDE 6000 rpm. E *vs.* Ag/10 mM $AgNO_3$ + 0.1 M TBAP in CH_3CN.

Two weak irreversible electrochemical waves at E_{pa} = 0.10 V and 0.58 V are observed in the positive range of potentials. The cathodic RDE voltammogram displays one wave at $E_{1/2}$ = -0.70 V, while on the anodic part of the RDE voltammogram, two successive oxidation waves can be found (Figure 7.5, right, curve b). The first anodic wave at $E_{1/2}$ = 0.06 V is of very low intensity and may correspond to the oxidation of a by-product, likely the starting Cu^{I} complex, present in a very small amount in solution. No electrochemical properties of trans-μ-1,2-peroxo-dicopper complexes have been previously reported, although Karlin and co-workers have very recently reported the CV curves of two μ-η^2:η^2 peroxo-dicopper(II) complexes.[26] However, based on the electrochemical data earlier reported for peroxo-bridged dinuclear cobalt complexes,[27,28] the irreversible cathodic wave has been assigned to the two-electron reduction of the Cu^{II} centers, resulting in the formation of unstable dicopper(I)-peroxo species, which quickly decompose. The main anodic wave was attributed to the one-electron oxidation

of the peroxo moiety, leading to the formation of the dicopper(II)-superoxo species, which is usually observed as an intermediate in the formation of trans-μ-1,2-peroxo-dicopper complexes. The assignment is fully consistent with the height of the RDE cathodic wave being twice the height of the second RDE anodic wave.

7.2.7 Catecholase activity of 1

The catalytic activity of **1** in the oxidation of commonly used model substrate 3,5-di-*tert*-butylcatechol ($DTBCH_2$) has been studied in acetonitrile saturated in dioxygen by monitoring the development of the UV-Vis band at 400 nm, corresponding to the absorption of the produced quinone (ε = 1900 $M^{-1}\cdot cm^{-1}$). Upon treating a 0.25 mM solution of the complex with 100 equivalents of $DTBCH_2$, a turnover number of 36 has been determined after one hour. The reaction follows a Michaelis-Menten behavior. The reaction rate in acetonitrile has been determined from the slope of trace at 400 nm in the first 20 minutes of the reaction, and a Lineweaver-Burk treatment gave V_{max} = 1.3×10^{-6} $M\cdot s^{-1}$ and K_M = 4.9 mM (Figure 7.6).

The utilization of other catechols with higher oxidation potentials, such as 3-fluorocatechol (3-FC), 3-nitrocatechol and tetrachlorocatechol showed that **1** catalyzes the oxidation of 3-FC, but fails to oxidize the latter two substrates. The catalytic reaction in the case of 3-FC proceeds, however, very slowly (*e.g.* one equivalent of quinone was formed after 20 min of reaction), which makes a more detailed kinetic analysis dispensable.

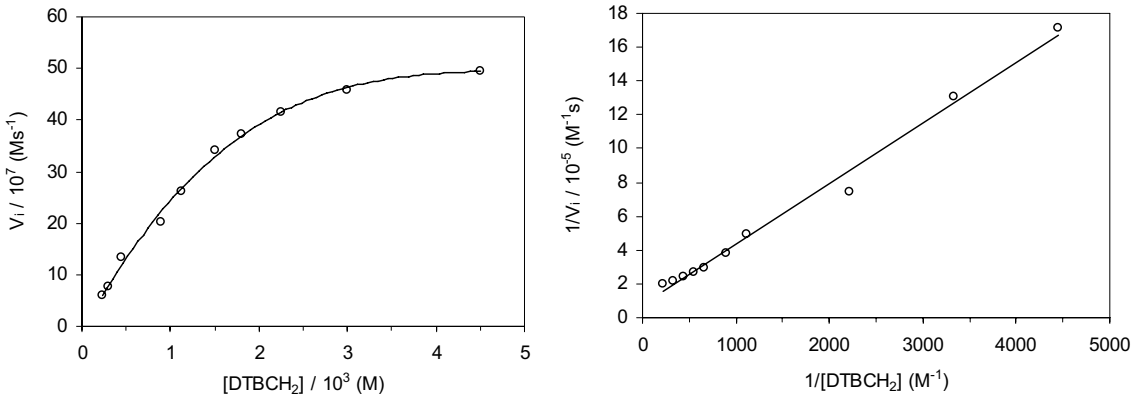

Figure 7.6. Plot of the initial reaction rates determined from the slope of trace at 400 nm in the first 20 minutes *vs.* substrate concentration, indicating substrate saturation behavior (left), and reciprocal Lineweaver-Burk plot (right).

7.2.8 Interaction of 1 with catechol substrates in anaerobic conditions

As shown previously by Krebs and co-workers,[29] the natural *met* form of catechol oxidase reacts with one equivalent of catechol stoichiometrically in anaerobic conditions, producing one equivalent of the corresponding quinone. A stoichiometric

oxidation of catechol has also been proposed or observed as a first step in the catalytic oxidation of catechols by copper(II) complexes.[6,12,30-32] Therefore the interaction of **1** with two model substrates, $DTBCH_2$ and 3-FC, has been investigated. The interaction of **1** with $DTBCH_2$ was evaluated by means of UV-Vis spectroscopy and electrochemically and its interaction with 3-FC from ^{19}F NMR spectroscopy experiments.

Upon addition of $DTBCH_2$ to 0.25 mM solution of **1** in acetonitrile under anaerobic conditions, one equivalent of the corresponding quinone is produced in a fast stoichiometric reaction along with the reduced species **2** (Figure 7.7). This can be evidenced from the disappearance of the CT band at 350 nm and the d-d band of the Cu^{II} ions, and the appearance of a new band at 400 nm, characteristic of the formed quinone. Two isosbestic points at 398 and 600 nm indicate the presence of two absorbing species in solution. As the reaction proceeds too fast to obtain the reliable values of the initial reaction rates, no detailed kinetic analysis could be performed. It is however obvious that the rates increase with the increase in the substrate concentration. The formation of DTBQ upon anaerobic interaction of **1** with $DTBCH_2$ has also been confirmed electrochemically. The addition of an excess of $DTBCH_2$ to a solution of **1** in acetonitrile leads to the development of a new RDE wave at $E_{1/2}$ = -0.88 V, corresponding to the two-electron reduction of the formed DTBQ (Figure 7.4, right, curve b).

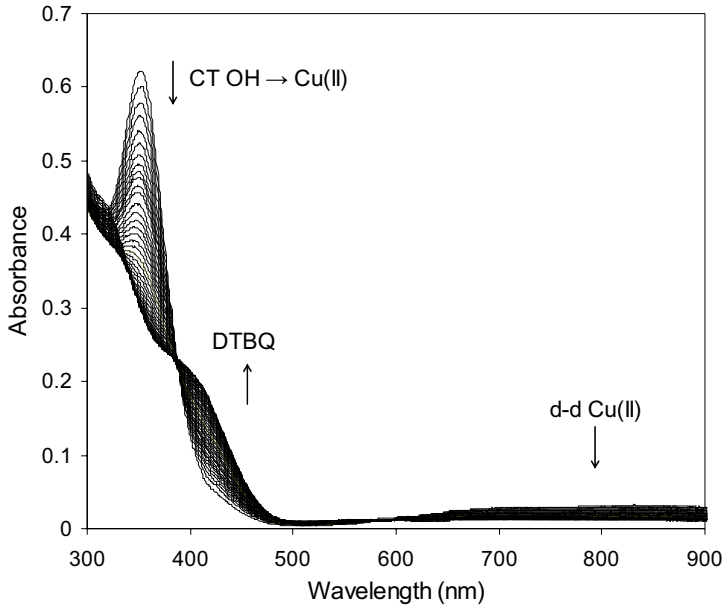

Figure 7.7. Changes in the UV-Vis spectra of **1** (CH_3CN, 2.5×10^{-4} M, dry glove box) upon addition of 3 molar equivalents of $DTBCH_2$ (spectra recorded every 5 seconds, l = 0.5 cm).

The anaerobic interaction of **1** with 3-FC, followed by UV-Vis spectroscopy, also revealed the formation of a very small amount of *o*-quinone. It appears to be much more difficult to oxidize 3-FC, which is in agreement with its higher oxidation potential in comparison with $DTBCH_2$. In fact, even in the presence of a large excess (60 molar

equivalents) of 3-FC, less than one equivalent of quinone was produced. The most direct proof of the quinone formation was obtained by means of ^{19}F NMR spectroscopy. Pure 3-FC exhibits one peak at 26.28 ppm in the ^{19}F NMR spectrum and the gradual addition of 3-FC to a solution of **1** in anaerobic conditions gives rise to a single new peak at 40.14 ppm, corresponding to the 3-fluoroquinone. The intensity of this peak was found to increase significantly in time upon addition of dioxygen, with a concomitant diminution of the original 3-FC peak. It has to be mentioned that no other peaks due to potential reaction intermediates, could be detected in the spectrum.

7.2.9 Interaction of 3 with catechol and phenolic substrates

Relatively few examples of the interaction of peroxo-dicopper(II) species with catechol substrates are described in the literature. Kitajima *et al.* reported the oxidative C-C coupling of $DTBCH_2$ by a μ-η^2:η^2 peroxo complex, resulting in the formation of diphenoquinones.[33] Interestingly, no formation of *o*-benzoquinone was observed, unless exogenous dioxygen was introduced into the reaction mixture. Casella and co-workers reported a stoichiometric oxidation of $DTBCH_2$ to DTBQ by a μ-η^2:η^2 peroxo-dicopper complex.[34] The same type of reactivity was observed by Stack and co-workers for a bis-μ-oxo-dicopper core.[35] The oxidation of $DTBCH_2$ by μ-η^2:η^2-peroxo and bis-μ-oxo-dicopper complexes was also reported by Tolman and co-workers[36] with isolation of mononuclear copper(II)-semiquinonate complexes as a sole product of the reaction, the (per)oxo-dicopper species being generated by reaction of two essentially mononuclear Cu^I molecules with dioxygen. Rockcliffe and Martell also reported a number of examples of the stoichiometric oxidation of catechols to the respective quinones or dicarboxylic acids involving various dicopper-dioxygen complexes.[31,37-39] Unfortunately, these authors did not provide detailed information concerning the structure of the peroxo species. Although the end-on dioxygen-binding mode was proposed based on the results of molecular modeling,[40] the UV-Vis spectroscopic data,[38,40] reported by the authors, as well as the overall reactivity of the described peroxo species[39,41] suggest that dioxygen is bound in the μ-η^2:η^2 mode. However, the oxidation of catechols by end-on peroxo-dicopper complexes has not been reported before, although the deprotonation of tetrachlorocatechol upon reaction with end-on trans-μ-1,2-peroxo-dicopper species has been evidenced by Comba and co-workers.[5,42]

The anaerobic interaction of **3** (*in situ*) with catechol has been studied spectrophotometrically at -40 °C in acetonitrile solution. The changes in the UV-Vis spectrum upon addition of one equivalent of catechol to a 0.25 mM solution of **3** are shown in Figure 7.8 (left). The disappearance of the peaks at 523 nm and 617 nm along with the development of the absorbance at 400 nm corresponds to the stoichiometric oxidation of the catechol substrate by **3**, leading to DTBQ (dotted line, Figure 7.8, left). The bubbling of dioxygen through the solution after completion of the reaction resulted in only a slight increase of the absorptions at 523 nm and 617 nm, indicating that the

trans-μ-1,2-peroxo core could not be restored. This suggests that the copper(II) ions are not reduced upon interaction with the substrate; thus, the oxidation of the substrate is likely to be performed by the peroxo moiety. Upon addition of an excess of $DTBCH_2$ to **3** in the presence of dioxygen, a catalytic oxidation of catechol takes place.

The mechanism of the catechol oxidation by **3** is of interest. Taking into account the basic nature of the end-on peroxo moiety, it can be proposed that in the first place the catechol acts as an acid toward **3**. This assumption is also supported by the earlier reports on the observed deprotonation of catechols and phenols after reaction with trans-μ-1,2-peroxo-dicopper cores.[5,42] Therefore the interaction of **3** with the deuterated analogue of $DTBCH_2$, in which the protons of the phenol groups are substituted with deuterium ($DTBCD_2$), has been studied. As can be seen from Figure 7.8 (left), the oxidation process clearly proceeds in two steps. First, the characteristic absorbencies of the peroxo-dicopper(II) species at 523 nm and 617 nm gradually disappears along with the appearance of the new peak at 342 nm. The isosbestic point at 440 nm indicates the presence of two species in solution. Second, the peak at 400 nm develops, indicating the formation of one equivalent of the quinone. The apparent reaction rate constant of the first process k^1_{obs} is 0.04 s^{-1} for $DTBCD_2$, whereas for non-deuterated $DTBCH_2$ the reaction is too fast to allow the determination of the reaction rate constant. For the second process, the reaction rate constant k^2_{obs} of 0.11 s^{-1} could be determined for both non-deuterated and deuterated substrate. Thus, on the second step of the reaction, no kinetic isotopic effect is observed, whereas a proton is obviously transferred on the first step. It can thus be proposed that initially the protonation of the peroxo core occurs along with the binding of the deprotonated substrate to the metal center, resulting in the formation of a ternary complex of a formal composition [Cu_2([22]py4pz)(O-O-H)-substrate]. The second step involves the oxidation of the bound catecholate by the peroxide moiety, which is thus independent on the proton/deuterium exchange. The interaction of **3** with the less reactive 3-fluorocatechol, the utilization of which stabilizes the formed hydroperoxo-dicopper(II)-substrate intermediate (**4**), has also been studied. The product **4**, formed upon treatment of **3** with one molar equivalent of 3-FC in acetonitrile, is characterized by the peak at 342 nm (ε =3960 $M^{-1}\cdot cm^{-1}$) in the UV-Vis spectrum and remains stable for at least 15 minutes at -40 °C. Its resonance Raman spectrum is characterized by the peak at 851 cm^{-1}, corresponding to a ν(O-O) stretching (Figure 7.2, right, curve B). The protonation thus increases the frequency of the O-O stretching in comparison to the original peroxo-dicopper(II) complex **3**, similarly to earlier reported results by Solomon *et al.*[43] The UV-Vis and resonance Raman spectroscopic characteristics of **4** are very close to the values earlier reported for other μ-1,1-hydroperoxo-copper(II) complexes;[44] furthermore, similarly to such complexes,[45] species **4** is EPR-silent. Thus, based on the spectroscopic data, the formation of μ-1,1-hydroperoxo-dicopper(II) intermediate upon reaction of **3** with catechol can be tentatively suggested. It should be noted that the formation of a hydroperoxo

intermediate has also been evidenced by Karlin *et al.*[24] in the reaction of trans-μ-1,2-peroxo-dicopper complexes with 2,4-di-*tert*-butylphenol.

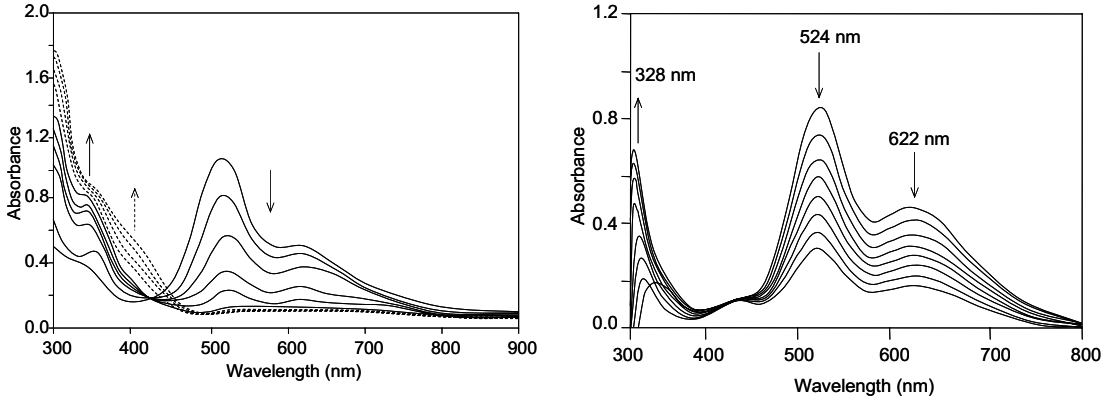

Figure 7.8. Left: changes in the UV-Vis spectrum upon addition of one equivalent of $DTBCD_2$ to a solution of **3** in anaerobic conditions (*in situ*, CH_3CN, 2.5×10^{-4} M, -40 °C). Solid lines: the spectra recorded each 0.2 min after $DTBCD_2$ addition to **3**. The dotted lines correspond to the gradual formation of one equivalent of DTBQ. For clarity, only the spectra recorded after 3.0, 6.0, 11.0 and 16.0 minutes are shown. Right: changes in the UV-Vis spectrum of **3** upon addition of one equivalent of sodium 4-carbomethoxyphenolate (2.5×10^{-4} M, acetone, -60 °C).

The interaction of **3** with sodium 4-carbomethoxyphenolate (a commonly used phenolic substrate) does not result in the hydroxylation of the aromatic ring (monophenolase activity). Earlier, Karlin and co-workers have pointed out the differences in reactivities between trans-μ-1,2-peroxo and μ-η^2:η^2 peroxo complexes.[24] While the former complexes are basic/nucleophlic in nature, the latter complexes display electrophilic properties. Recently, an electrophilic aromatic substitution mechanism has been proposed for the hydroxylation of phenols to the respective catechols by μ-η^2:η^2 peroxo complexes.[46] It includes a rate-determining electrophilic attack of the μ-η^2:η^2 peroxo core, while the oxygenation of the substrate (C-O bond formation) happens simultaneously with the O-O bond cleavage of the peroxo intermediate. Thus, the inability of **3** to hydroxylate a phenol substrate agrees with its nucleophilic character and is consistent with the earlier proposed mechanism of the phenolase activity of peroxo-dicopper complexes. The binding of the phenolate to the metal centers could, however, be confirmed, as the peroxo absorptions in the UV-Vis spectrum decreased with the addition of phenolate (Figure 7.8, right) and could not be restored upon purging the reaction mixture with pure dioxygen. At the same time, the peak at 328 nm gradually develops in the spectrum, which probably corresponds to the CT band from the coordinated phenolate to the copper(II) ions, as it is consistent with the spectroscopic characteristics observed for the reaction of dicopper(II) complexes with kojic acid,[47] and for copper(I)-phenolate adducts.[48]

7.2.10 Mechanistic considerations

On the basis of the results described above, a mechanism for the catechol oxidation by **1**, as depicted in Figure 7.9, can be proposed.

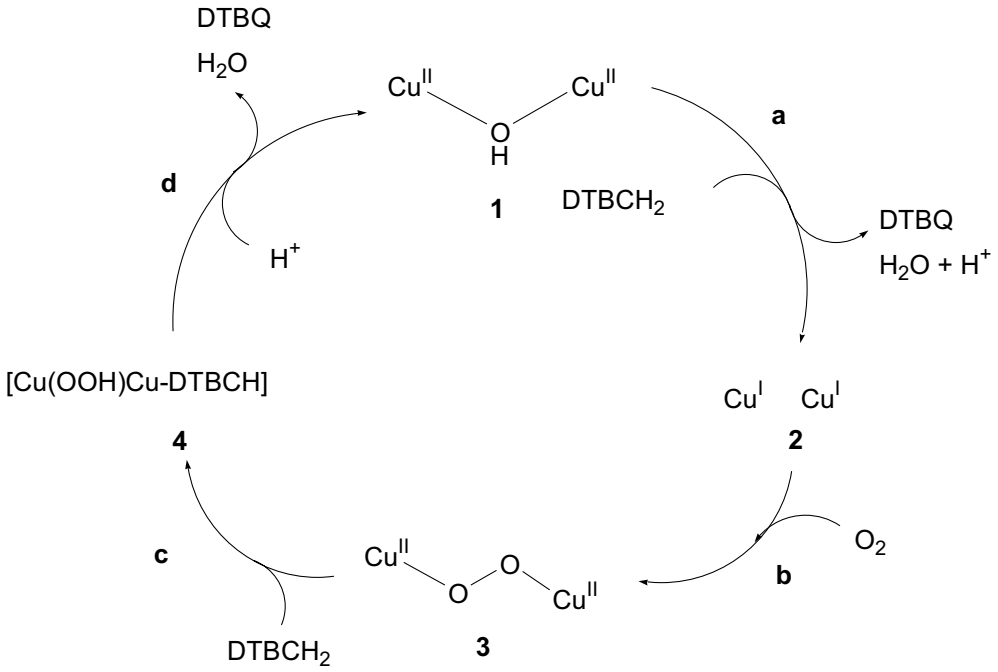

Figure 7.9. Proposed mechanism for the oxidation of 3,5-di-*tert*-butylcatechol by **1**. The complexes **1** and **2** are characterized crystallographically, the peroxo-dicopper(II) intermediate **3** is characterized by UV-Vis and resonance Raman spectroscopy.

In the first stage of the reaction, a stoichiometric oxidation of catechol by **1** takes place (step **a**, Figure 7.9). This step does not require the presence of dioxygen. At the second stage, the dicopper(I) complex **2**, which is formed upon $DTBCH_2$ oxidation by **1**, reacts with dioxygen to form the trans-μ-1,2-peroxo-dicopper(II) species **3** (step **b**). This species oxidizes a second equivalent of catechol in stoichiometric reaction through a two-electron transfer from the catechol to the peroxide moiety. The reaction proceeds in two steps: the proton transfer from the substrate to the nucleophilic peroxo core (step **c**), and the oxidation of the bound catecholate (step **d**). As suggested earlier by Casella *et al.*,[47] the steps **b**-**d** appear to determine the overall catalytic efficiency of **1**, as step **a** is too fast to be considered as a rate-determining step. After the quinone molecule is released, the complex **1** is regenerated, and the catalytic cycle can continue, as shown in Figure 7.9. Two equivalents of quinone are thus generated per one catalytic cycle. This mechanism is in fact very similar to the mechanisms earlier proposed by Rockcliffe *et al.*[31] and Casella and co-workers[49] for dinuclear Cu^{II} complexes, and by Krebs and co-workers for catechol oxidase.[29,50] Two major differences between the present mechanism and those earlier described should though be pointed out. The first one is the structure of the peroxo-dicopper intermediate. Whereas the formation of a μ-η^2:η^2 peroxo-dicopper intermediate was shown for catechol oxidase,[50,51] Casella and co-workers reported the

formation of either μ-η^2:η^2 peroxo or μ-oxo-dicopper species upon reaction of dicopper(I) species with dioxygen, dependent on the ligand structure.[6,34] In the present case, however, dioxygen is clearly bound in a trans-μ-1,2 fashion. The second difference concerns the actual mechanism of catechol oxidation by peroxo-dicopper species. Whereas Krebs and co-workers have proposed the simultaneous binding of dioxygen and the substrate to the deoxy form of catechol oxidase prior to the quinone formation,[29,50] a two-step oxidation mechanism of the substrate by the formed peroxo-dicopper(II) core with the formation of the hydroperoxo-dicopper intermediate takes place in the present case.

In conclusion, a mechanism for the catechol oxidation by the dicopper(II) complex bearing a hydroxide bridge between the metal ions is proposed, with the adequate characterization of the reduced dicopper(I) complex and dicopper(II)-dioxygen adduct. The proposed mechanism closely resembles the earlier mechanism published by Krebs and co-workers of catechol oxidation by the natural enzyme, although the binding mode of the substrate to the dicopper centers unfortunately remains unclear.[29] It should be noted that in this chapter the first example of catechol oxidation by a trans-μ-1,2-peroxo-dicopper species is reported. Remarkably, this species is able to oxidize catechols (catecholase activity), but is not able to perform the hydroxylation of the *o*-position of phenols (tyrosinase activity). Although the formation of μ-η^2:η^2 peroxo species has been evidenced by the treatment of catechol oxidase (*met* form) isolated from *Lycopus europaeus* and *Populus nigra* with H_2O_2, and trans-μ-1,2-peroxo intermediates have never been observed in the natural systems, it is interesting to note that the difference in behavior towards phenol and catechol substrates can in fact be dependent on the structure of the copper-dioxygen adduct. Furthermore, Karlin and co-workers have reported a very rapid conversion of a trans-μ-1,2-peroxo-dicopper intermediate into a μ-η^2:η^2 final species, and suggested that the "end-on" species may initially form upon dioxygen binding by the type-3 copper proteins, due to the long distance between the metal ions in the reduced dicopper(I) core, which may rapidly interconvert into "side-on" species.[52] It is thus fascinating to notice the possible existence of end-on peroxo-dicopper moieties in living systems and the possibility that the reactivity towards different substrates can be tuned by the type of dicopper-dioxygen adduct. Although these assumptions are largely speculative in natural enzymes, future studies on dicopper-dioxygen model systems and their reactivity would be very beneficial in order to shed light on the interpretation of the mechanisms of monophenolase and diphenolase activity by type-3 copper proteins.

7.3 Experimental Section

7.3.1 Materials and Methods

All starting materials were commercially available and used as purchased, unless stated otherwise. The macrocyclic ligand [22]py4pz and [Cu_2([22]py4pz)(μ-

OH)](ClO$_4$)$_3$·H$_2$O (**1**) were synthesized as previously described [15,53] (see also Chapter 6). The ligand field spectra in solution were recorded on a Varian Cary 50 Scan UV-Vis spectrophotometer (l = 1 cm), and on a Zeiss MCS500 Diode-Array Spectrometer (l = 0.5 cm). X-band electron paramagnetic resonance (EPR) measurements were performed at 100 K on 1 mM frozen solutions in acetonitrile on a Bruker ESP 300E spectrometer operating at 9.4 GHz (X-band). Resonance Raman spectra were recorded on a Dilor XY multichanel spectrometer. The sample was kept in acetonitrile at -70 °C. As excitation source a coherent Ar laser (514.532 nm) was used. The spectra were run with a laser power of 30 mW and an acquisition time of 2×1800 s. ^{1}H and ^{19}F NMR spectra were recorded on a Bruker Avance 300 spectrometer at 25 °C. Chemical shifts were referenced to CD_3CN as internal reference and to C_6F_6 as external reference, respectively. The deprotonation constants of **1** were determined spectrophotometrically at 25 °C in a 2.5×10^{-4} M solution in a DMSO:H$_2$O mixture (1:9), monitoring the UV-vis band at 350 nm, and using the method of Schwarzenbach.[54] The ionic strength was maintained constant with a 0.01 M solution of $NaNO_3$. The electrochemical behavior of the complexes was investigated in a 0.1 M solution of tetra-*n*-butylammonium perchlorate (TBAP) in acetonitrile using a EGG 273 potentionstat coupled with a Kipp&Zonen x-y recorder. The experiments were performed at room temperature in a three-compartment cell. Potentials are referred to an Ag/10 mM $AgNO_3$ + CH_3CN + 0.1 M TBAP reference electrode. The working electrode was a platinum disk of 5 mm diameter for the cyclic voltammetry (CV, 0.1 V·s^{-1}) experiments or 3 mm diameter for the rotating disk electrode (RDE, 600 rpm) voltammetry experiments. The working electrode was polished with 1 μm diamond paste prior to each recording.

7.3.2 Syntheses of coordination compounds

[Cu$_2$([22]py4pz)](ClO4)$_2$·2CH$_3$OH (2): In a glove box, a solution of [Cu(CH_3CN)$_4$]ClO$_4$ (65 mg, 0.20 mmol) in 2 ml of dry methanol was added to a suspension of [22]py4pz (58 mg, 0.10 mmol) in the same solvent. The diffusion of diethyl ether into the resulting solution led to the appearance of small pale yellow crystals, suitable for X-ray diffraction analysis. They were found to be very sensitive to air and moisture and could be stored only in an inert atmosphere. ^{1}H-NMR (CD_3CN, 300 MHz, ppm): 8.57 (d, 2H, 6'H-py, J = 5.1 Hz), 7.86 (td, 2H, 4'H-py, J = 7.7 Hz, J = 1.7 Hz), 7.45 (s, 4H, 5'H-pz, broad), 7.39 (m, 8H, 3'H-py +5'H-py), 6.14 (s, 4H, 4'H-pz, broad), 4.61 (s, 8H, pz-CH$_2$-CH$_2$-pz, broad), 3.79 (s, 4H, N-CH$_2$-py, broad), 3.66 (s, 8H, N-CH$_2$-pz, broad). ESI-MS, m/z: z = 2, [Cu$_2$([22]py4pz)]$^{2+}$ = 358.

Trans-μ-1,2-peroxo-dicopper complex 3 derived from 2: Trans-μ-1,2-peroxo-dicopper complex **3** was prepared *in situ* upon bubbling dioxygen into a preliminary cooled to -40 °C 2.5×10^{-4} M solution of [Cu$_2$([22]py4pz)](ClO$_4$)$_2$ (**2**) in acetonitrile. UV-Vis (CH_3CN): λ/nm (ε/M^{-1}·cm^{-1}): 523 (4320), 617 (2212). Resonance Raman (CH_3CN, -70 °C): 840 cm^{-1} (O-O stretching), 510 cm^{-1} (Cu-O stretching).

7.3.3 Catecholase activity studies

The catecholase activity of **1** was evaluated by reaction with 3,5-di-*tert*-butylcatechol ($DTBCH_2$) at 25 ºC. The absorption at 400 nm, characteristic of the formed quinone, 3,5-di-*tert*-butyl-*o*-benzoquinone (DTBQ), was measured as a function of time. The experiments were run in acetonitrile saturated with dioxygen. The kinetic parameters were determined for 4.5×10^{-5} M solutions of the complex and 0.225–4.5 mM solutions of the substrate. In a typical catalytic experiment, 3 ml of a solution of **1** were placed in a 1 cm path-length cell, and the solution was saturated with dioxygen. Afterwards 75 µl of the substrate solution were added. After thorough stirring, the changes in UV-Vis spectra were recorded during 30 min.

The interaction of **3** with $DTBCH_2$, spectrophotometrically monitored, was carried out under argon at -40 °C in acetonitrile by adding 25 µl of a 0.4 M solution of $DTBCH_2$ (10 µmol) to 40 ml of a 2.5×10^{-4} M solution of **3** (10 µmol), prepared *in situ*. The phenol oxidation experiments (tyrosinase activity) were carried out by adding a solution of sodium 4-carbomethoxyphenolate (two or more equivalents) in dry acetone to a cooled to -60 ˚C solution of either **3** or **2** (0.1-0.3 mM, both compounds prepared *in situ*), in dry dichloromethane, acetone or acetonitrile.[47,48,55] Dioxygen bubbling through the solution was continued (in case of **2**, dioxygen was introduced into the solution immediately after the substrate was added), and the reaction mixture was stirred at low temperature in dioxygen-saturated atmosphere. After at least four hours a sample (1 ml) was withdrawn from the reaction mixture and immediately quenched with H_2SO_4. After evaporation of the solvent, 1 ml of H_2O was added, and the resulting solution was analyzed by HPLC, using a Supelco LC18 semipreparative column (250×10 mm). Elution was carried out at 5 ml·min^{-1} starting with water containing 0.1% trifluoroacetic acid for 4 min, followed by a linear gradient from 0% to 100% acetonitrile containing 0.1% trifluoroacetic acid during 20 min. Spectrophotometric detection of the HPLC elution profile in the range 200-650 nm was performed with a Jasco MD-1510 diode array instrument.[56]

7.3.4 X-ray Crystallographic Measurements

The crystal of **2** was mounted on a Enraf-Nonius Kappa CCD diffractometer using a graphite monochromator (λ (Mo K_α): 0.71073 Å). The structure was solved by direct methods and refined using the TEXSAN software.[57] Empirical formula: $[Cu_2C_{32}H_{37}N_{12}]\cdot(ClO_4)_2\cdot(CH_3OH)_2$, Fw = 978.79, colorless block (0.25 mm×0.20 mm×0.18 mm), monoclinic, space group *P21/n*, a = 13.416(4) Å, b = 20.491(20) Å, c = 15.013(5) Å, $\alpha = \gamma = 90°$, β = 98.48(4)°, V = 4082(4) Å^3, Z = 4, $\rho_{calc.}$ = 1.593 g·cm^{-3}, μ = 1.244 mm^{-1}. A total of 52771 reflections, of which 11173 were independent [R(int) = 0.07176], were collected in the range $3 \leq 2\theta \leq 30°$. All non-hydrogen atoms were refined with anisotropic thermal parameters. Hydrogen atoms were generated in

idealized positions, riding on the carrier atoms, with isotropic thermal parameters. Final cycle refinement converged to $R(F) = 0.0675$ and $wR2 = 0.10965$.

Crystallographic data (without structure factors) for the structure of **2** have been deposited with the Cambridge Crystallographic Data Centre as supplementary publication no. CCDC-269469. Copies of the data can be obtained free of charge from the CCDC (12 Union Road, Cambridge CB2 1EZ, UK; tel: (+44) 1223-336-408; fax: (+44) 1223-336-003; e-mail: deposit@ccdc.cam.ac.uk).

7.4 References

(1) Selmeczi, K.; Reglier, M.; Speier, G.; Peintler, G. *React. Kinet. Catal. Lett.* **2004**, *81*, 143-151.
(2) Selmeczi, K.; Reglier, M.; Giorgi, M.; Speier, G. *Coord. Chem. Rev.* **2003**, *245*, 191-201.
(3) Gao, J.; Reibenspies, J. H.; Martell, A. E. *Inorg. Chim. Acta* **2003**, *346*, 67-75.
(4) Ackermann, J.; Meyer, F.; Kaifer, E.; Pritzkow, H. *Chem. Eur. J.* **2002**, *8*, 247-258.
(5) Börzel, H.; Comba, P.; Pritzkow, H. *Chem. Commun.* **2001**, 97-98.
(6) Granata, A.; Monzani, E.; Casella, L. *J. Biol. Inorg. Chem.* **2004**, *9*, 903-913.
(7) Louloudi, M.; Mitopoulou, K.; Evaggelou, E.; Deligiannakis, Y.; Hadjiliadis, N. *J. Mol. Cat. A* **2003**, *198*, 231-240.
(8) Merkel, M.; Möller, N.; Piacenza, M.; Grimme, S.; Rompel, A.; Krebs, B. *Chem. Eur. J.* **2005**, *11*, 1201-1209.
(9) Mukherjee, J.; Mukherjee, R. *Inorg. Chim. Acta* **2002**, *337*, 429-438.
(10) Monzani, E.; Battaini, G.; Perotti, A.; Casella, L.; Gullotti, M.; Santagostini, L.; Nardin, G.; Randaccio, L.; Geremia, S.; Zanello, P.; Opromolla, G. *Inorg. Chem.* **1999**, *38*, 5359-5369.
(11) Monzani, E.; Quinti, L.; Perotti, A.; Casella, L.; Gulotti, M.; Randaccio, L.; Geremia, S.; Nardin, G.; Faleschini, P.; Tabbi, G. *Inorg. Chem.* **1998**, *37*, 553-562.
(12) Than, R.; Feldmann, A. A.; Krebs, B. *Coord. Chem. Rev.* **1999**, *182*, 211-241.
(13) Torelli, S.; Belle, C.; Gautier-Luneau, I.; Pierre, J. L.; Saint-Aman, E.; Latour, J. M.; Le Pape, L.; Luneau, D. *Inorg. Chem.* **2000**, *39*, 3526-3536.
(14) Torelli, S.; Belle, C.; Hamman, S.; Pierre, J. L.; Saint-Aman, E. *Inorg. Chem.* **2002**, *41*, 3983-3989.
(15) Koval, I. A.; van der Schilden, K.; Schuitema, A. M.; Gamez, P.; Belle, C.; Pierre, J.-L.; Luken, M.; Krebs, B.; Roubeau, O.; Reedijk, J. *Inorg. Chem.* **2005**, *44*, 4372-4382.
(16) Gerdemann, C.; Eicken, C.; Krebs, B. *Acc. Chem. Res.* **2002**, *35*, 183-191.
(17) Bol, J. E.; Driessen, W. L.; Ho, R. Y. N.; Maase, B.; Que, L.; Reedijk, J. *Angew. Chem. Int. Ed. Engl.* **1997**, *36*, 998-1000.
(18) Addison, A. W.; Rao, T. N.; Reedijk, J.; van Rijn, J.; Verschoor, G. C. *J. Chem. Soc., Dalton Trans.* **1984**, 1349-1356.
(19) Liu, W.; Thorp, H. H. *Inorg. Chem.* **1993**, *32*, 4102-4105.
(20) Baldwin, M. J.; Ross, P. K.; Pate, J. E.; Tyeklár, Z.; Karlin, K. D.; Solomon, E. I. *J. Am. Chem. Soc.* **1991**, *113*, 8671-8679.
(21) Solomon, E. I.; Tuczek, F.; Root, D. E.; Brown, C. A. *Chem. Rev.* **1994**, *94*, 827-856.
(22) Mirica, L. M.; Ottenwaelder, X.; Stack, T. D. P. *Chem. Rev.* **2004**, *104*, 1013-1045.
(23) Gamez, P.; Koval, I. A.; Reedijk, J. *Dalton Trans.* **2004**, 4079-4088.
(24) Paul, P. P.; Tyeklár, Z.; Jacobson, R. R.; Karlin, K. D. *J. Am. Chem. Soc.* **1991**, *113*, 5322-5332.
(25) Reim, J.; Krebs, B. *J. Chem. Soc., Dalton Trans.* **1997**, 3793-3804.
(26) Shearer, J.; Zhang, C. X.; Zakharov, L. N.; Rheingold, A. L.; Karlin, K. D. *J. Am. Chem. Soc.* **2005**, *127*, 5469-5483.
(27) Ghiladi, M.; Gomez, J. T.; Hazell, A.; Lumtscher, J.; McKenzie, C. J. *Dalton Trans.* **2003**, 1320-1325.
(28) Harris, W. R.; McLendon, G. L.; Martell, A. E.; Bess, R. C.; Mason, M. *Inorg. Chem.* **1980**, *19*, 21-26.
(29) Eicken, C.; Krebs, B.; Sacchettini, J. C. *Curr. Opin. Struct. Biol.* **1999**, *9*, 677-683.
(30) Gupta, M.; Mathur, P.; Butcher, R. J. *Inorg. Chem.* **2001**, *40*, 878-885.
(31) Rockcliffe, D. A.; Martell, A. E. *J. Mol. Catal. A* **1995**, *99*, 101-114.
(32) Chyn, J.-P.; Urbach, F. L. *Inorg. Chim. Acta* **1991**, *189*, 157-163.
(33) Kitajima, N.; Koda, T.; Iwata, Y.; Moro-oka, Y. *J. Am. Chem. Soc.* **1990**, *112*, 8833-8839.
(34) Santagostini, L.; Gulotti, M.; Monzani, E.; Casella, L.; Dillinger, R.; Tuczek, F. *Chem. Eur. J.* **2000**, *6*, 519-522.

(35) Mahadevan, V.; Dubois, L.; Hedman, B.; Hodgson, K. O.; Stack, T. D. *J. Am. Chem. Soc.* **1999**, *121*, 5583-5584.
(36) Berreau, L. M.; Mahapatra, S.; Halfen, J. A.; Houser, R. P.; Young, V. G.; Tolman, W. B. *Angew. Chem. Int. Ed. Engl.* **1999**, *38*, 207-210.
(37) Rockcliffe, D. A.; Martell, A. E. *J. Chem. Soc., Chem. Commun.* **1992**, 1758-1760.
(38) Rockcliffe, D. A.; Martell, A. E.; Reibenspies, J. H. *J. Chem. Soc., Dalton Trans.* **1996**, 167-175.
(39) Rockcliffe, D. A.; Martell, A. E. *J. Mol. Cat. A* **1996**, *106*, 211-221.
(40) Rockcliffe, D. A.; Martell, A. E. *J. Mol. Catal. A* **1995**, *99*, 87-99.
(41) Rockcliffe, D. A.; Martell, A. E. *Inorg. Chem.* **1993**, *32*, 3143-3152.
(42) Börzel, H.; Comba, P.; Hagen, K. S.; Kerscher, M.; Pritzkow, H.; Schatz, E.; Schindler, S.; Walter, O. *Inorg. Chem.* **2002**, *41*, 5440-5452.
(43) Root, D. E.; Mahroof-Tahir, M.; Karlin, K. D.; Solomon, E. I. *Inorg. Chem.* **1998**, *37*, 4838-4848.
(44) Itoh, K.; Hayashi, H.; Furutachi, H.; Mathumoto, T.; Nagamoto, S.; Tosha, T.; Terada, S.; Fujinami, S.; Suzuki, F.; Kitagawa, T. *J. Am. Chem. Soc.* **2005**, *127*, 5212-5223, and references therein.
(45) Karlin, K. D.; Ghosh, P.; Cruse, R. W.; Meyer, G. J.; Farooq, A.; Gultneh, Y.; Jacobson, R. R.; Blackburn, N. J.; Strange, R. W.; Zubieta, J. *J. Am. Chem. Soc.* **1988**, *110*, 6769-6780.
(46) Itoh, S.; Kumei, H.; Taki, M.; Nagamoto, S.; Kitagawa, T.; Fukuzumi, S. *J. Am. Chem. Soc.* **2001**, *123*, 6708-6709.
(47) Battaini, G.; Monzani, E.; Casella, L.; Santagostini, L.; Pagliarin, R. *J. Biol. Inorg. Chem.* **2000**, *5*, 262-268.
(48) Casella, L.; Monzani, E.; Gulotti, M.; Cavagnino, D.; Cerina, G.; Santagostini, L.; Ugo, R. *Inorg. Chem.* **1996**, *35*, 7516-7525.
(49) Martell, A. E.; Motekaitis, R. J.; Menif, R.; Rockcliffe, D. A.; Llobet, A. *J. Mol. Cat. A* **1997**, *117*, 205-213.
(50) Klabunde, T.; Eicken, C.; Sacchettini, J. C.; Krebs, B. *Nat. Struct. Biol.* **1998**, *5*, 1084-1090.
(51) Rompel, A.; Fischer, H.; Meiwes, D.; Buldt Karentsopoulos, K.; Dillinger, R.; Tuczek, F.; Witzel, H.; Krebs, B. *J. Biol. Inorg. Chem.* **1999**, *4*, 56-63.
(52) Jung, B.; Karlin, K. D.; Zuberbühler, A. D. *J. Am. Chem. Soc.* **1996**, *118*, 3763-3764.
(53) Schuitema, A. M.; Aubel, P. G.; Koval, I. A.; Engelen, M.; Driessen, W. L.; Reedijk, J.; Lutz, M.; Spek, A. L. *Inorg. Chim. Acta* **2003**, *355*, 374-385.
(54) Schwarzenbach, G.; Schwarzenbach, K. *Helv. Chim. Acta* **1963**, *46*, 1390-1400.
(55) Schuitema, A. M. Ph.D. thesis, Leiden University, 2004.
(56) Battaini, G.; De Carolis, M.; Monzani, E.; Tuczek, F.; Casella, L. *Chem. Commun.* **2003**, 726-727.
(57) *TEXSAN, Single-Crystal Structure Analysis Software*. Molecular Structure Corporation: The Woodlands, TX, 1995